Journal of Neuroimmunology 367 (2022) 577874

Contents lists available at ScienceDirect

Journal of Neuroimmunology

journal homepage: www.elsevier.com/locate/jneuroim

Lesion-associated microglia and macrophages mediate corralling and react with massive phagocytosis for debris clearance and wound healing after LPS-induced dopaminergic depletion

P. Heman-Bozadas [a,b], C. Romero [a], P. Martínez-Remedios [a,1], I. Freitag [a,1], A. Frías [a], E. Saavedra-López [a], P.V. Casanova [a], M. Roig-Martínez [a], G.P. Cribaro [a], M.J. Rovirosa-Hernández [b], D. Hernandez-Baltazar [b,c], C. Barcia [a,*]

[a] Institut de Neurociències & Department of Biochemistry and Molecular Biology, School of Medicine & School of Biosciences, Universitat Autònoma de Barcelona, Barcelona, Spain
[b] Instituto de Neuroetología, Universidad Veracruzana, Xalapa, Veracruz, Mexico
[c] Cátedras CONACyT, Dirección Adjunta de Desarrollo Tecnológico e Innovación, Consejo Nacional de Ciencia y Tecnología. CDMX, Mexico

ARTICLE INFO

Keywords:
Parkinson's disease
Microglia
Macrophages
Lipopolysaccharide
Phagocytosis
Dopamine
Neurodegeneration
Experimental models

ABSTRACT

Neuroinflammation contributes to neuronal degeneration in Parkinson's disease (PD). However, how brain inflammatory factors mediate the progression of neurodegeneration is still poorly understood. Experimental models of PD have shed light on the understanding of this phenomenon, but the exploration of inflammation-driven models is necessary to better characterize this aspect of the disorder. The use of lipopolysaccharide (LPS) to induce a neuroinflammation-mediated neuronal loss is useful to induce reliable elimination of dopaminergic neurons. Nevertheless, how this model parallels the PD-like neuroinflammation is uncertain. In the present work, we used the direct LPS injection as a model inductor to eliminate dopaminergic neurons of the substantia nigra *pars compacta* (SNpc) in rats and reevaluated the inflammatory reaction. High-resolution 3D histological examination revealed that, although LPS induced a reliable elimination of SNpc dopaminergic neurons, it also generated a massive inflammatory response. This inflammation-mediated injury was characterized by corralling, a damaged parenchyma occupied by a vast population of lesion-associated microglia and macrophages (LAMMs) undertaking wound compaction and scar formation, surrounded by highly reactive astrocytes. LAMMs tiled the entire lesion and engaged in long-standing phagocytic activity to resolve the injury. Additionally, modeling LPS inflammation in a cell culture system helped to understand the role of phagocytosis and cytotoxicity in the initial phases of dopaminergic degeneration and indicated that LAMM-mediated toxicity and phagocytosis coexist during LPS-mediated dopaminergic elimination. However, this type of severe inflammatory-mediated injury, and subsequent resolution appear to be different from the ageing-related PD scenario where the architectural structure of the parenchyma is mostly preserved. Thus, the necessity to explore new experimental models to properly mimic the inflammatory compound observed in PD degeneration.

1. Introduction

Parkinson's disease (PD) is characterized by a dramatic loss of dopaminergic neurons of the substantia nigra *pars compacta* (SNpc) (Kalia and Lang, 2015; Przedborski, 2017). The cause of this neurodegeneration is still under scrutiny. Although the contribution of glial-mediated neuroinflammation is now generally accepted, many questions remain unanswered regarding the particular role of inflammatory mediators on dopaminergic neurons (Hirsch and Standaert, 2020). Thus, understanding neuroinflammatory response in PD is essential to design alternative therapeutic interventions (Charvin et al., 2018; Wang et al., 2015). For this to be elucidated, experimental models of parkinsonian-like neuroinflammation are necessary to understand the action of local glial cells, as well as potential infiltrated immune cells, on

* Corresponding author at: Department of Biochemistry and Molecular Biology, Institut de Neurociències, School of Medicine, Lab M2-107, Office M2-117, Universitat Autònoma de Barcelona, Bellaterra 08193, Barcelona, Spain.
E-mail address: carlos.barcia@uab.es (C. Barcia).
[1] These authors contributed equally to this work.

https://doi.org/10.1016/j.jneuroim.2022.577874
Received 8 June 2021; Received in revised form 17 March 2022; Accepted 19 April 2022
Available online 22 April 2022

neurons (Deng et al., 2020).

The SNpc of PD patients display several hallmarks of active inflammatory response such as microglial activation (McGeer et al., 1988) and reactive astrogliosis (Forno et al., 1992) in a relatively well preserved structure of the parenchyma. Well-established neurotoxic experimental PD models, such as MPTP or 6-OHDA (Akiyama and McGeer, 1989; Barcia et al., 2011; Czlonkowska et al., 1996), recapitulate the neuroinflammatory reaction observed in PD patients (McGeer et al., 1988), analogously to the incidentally intoxicated human MPTP cases (Langston et al., 1999). However, in these models, the effects of the neuroinflammatory response and neurotoxicity are hardly separable. For this reason, alternative models considering solely the inflammatory response are critical to understand its potential contribution to dopaminergic degeneration (Tufekci et al., 2011).

The gram-negative bacterial membrane compound lipopolysaccharide (LPS) has long been used to promote neuroinflammatory responses *in vivo* (Brown, 2019; Catorce and Gevorkian, 2016; Hoogland et al., 2015) and *in vitro* (Orihuela et al., 2016; Schmid et al., 2009). Particularly *in vitro*, together with IFN-γ, it is canonically used to skew cells of macrophage lineage to a proinflammatory phenotype (Shapouri-Moghaddam et al., 2018; Zhu et al., 2015). *In vivo*, the direct injection of LPS in the central nervous system (CNS) in rodents has commonly been used to study neuroinflammation, particularly as an inflammation-induced PD model when injected directly into dopaminergic areas, specifically the SNpc (Deng et al., 2020; Duty and Jenner, 2011). Inducing this proinflammatory phenotype in the CNS has been particularly useful to understand the harmful effects on neurons. Moreover, the hypothesis that bacterial-derived, LPS-mediated neuroinflammation could be behind PD pathogenesis makes this approach increasingly relevant (Brown, 2019). In fact, recent evidences point to unbalanced gut microbiome as a potential contributor of the PD-related inflammation (Romano et al., 2021), but how LPS or other membrane-bound bacterial components reach the brain is still to be determined (Wong, 2021).

It is clear that intranigral LPS injection generates reliable neuronal loss, which can be suitable for answering particular scientific questions (Deng et al., 2020), but whether the inflammation of this model is comparable to PD-like inflammation is still unclear.

In the present work, we revisited the neuroinflammatory response generated by the direct injection of LPS in the SNpc in a rat model of dopaminergic degeneration and analyzed in detail with cellular resolution the effects on the mesencephalic parenchyma. We observed that on the one hand, LPS-induced dopaminergic loss causes severe tissue damage characterized by microglial activation and massive macrophage infiltration enclosed in an astrocyte-mediated corralled lesion showing high phagocytic capacity of dopaminergic debris, wound compaction and scar formation. These results indicate that although dopaminergic loss is reproducible and reliable, the inflammation caused by the direct injection of LPS does not recapitulate the typical inflammatory response observed in ageing and PD.

2. Results

To revisit the effectiveness of LPS as a dopaminergic neurotoxin and potential experimental model for PD, first, we analyzed the consistency of a direct LPS injection inducing dopaminergic neuronal loss in the SNpc (Fig. 1A-C). We examined an early time window of three days to analyze the initial neuroinflammatory response and related neurodegeneration, and also at seven days to observe the potential recovery of the lesion. Precise intra-parenchymal LPS injection originated dopaminergic depletion in the targeted site, observable both three and seven days after the injection, with no apparent effect on the contralateral side (Fig. 1D). Mainly dopaminergic neurons were eliminated but, interestingly, non-dopaminergic neurons, quantified as $NeuN^+$ with no TH expression, also showed a similar percentage of reduction (Fig. 1 *E*-G) questioning the specificity and the particular vulnerability of dopaminergic neurons to this endotoxin. At seven days, both dopaminergic and non-dopaminergic neuronal loss seemed to be slightly higher, suggesting a progression of the neuronal degeneration.

Most importantly, LPS-induced dopaminergic neuronal loss was associated with a massive accumulation of lesion-associated microglia and macrophages (LAMMs), evidenced by the marker OX42 at the injection site (Fig. 2A, B). Reduction of dopaminergic area on the ipsilateral side was concomitant with the populating of a vast amount of $OX42^+$ cells compared with the contralateral side (Fig. 2B). This phenomenon could be seen in LPS-injected areas both at three and seven days after injection, whereas only scant levels of activation could be seen after saline injection (Fig. 2C). Higher resolution images of the $OX42^+$ cells in the SNpc revealed drastic morphological changes in LPS-injected parenchyma (Fig. 2C). Quantification of the number of $OX42^+$ cells in the SNpc shown a dramatic increase in LAMMs in the site of injection three days after LPS delivery. Moreover, this increase persisted at seven days, together with a mild increase observed on the contralateral side (Fig. 2D). Skeletonized $OX42^+$ cells from high-resolution images illustrate the representative morphological changes after LPS delivery. While sham and saline-injected areas show recognizable microglial morphology, LPS-injected areas show rounded-shape cells, compatible with vast monocyte infiltrate (Fig. 2E). Examination of sections, in fact, showed a massive population of $OX42^+$ cells around vascular structures in the SNpc area (Supplementary Fig. S1), suggesting the contribution of blood-infiltrated macrophages to the LAMM population at the injection site.

Importantly, since it is described that LAMM promote corralling in traumatic nervous system injuries (Zhou et al., 2020), we wanted to analyze whether this phenomenon also occurred in the LPS-mediated neuroinflammatory scenario. For this, we use antibodies for glial fibrillary acidic protein (GFAP) to detect reactive astrocytes in the mesencephalon sections. Microscopy images revealed that GFAP immunoreactivity was higher in the LPS injected hemisphere (Fig. 3 A), compared with the contralateral side. However, the core of the lesion showed reduced GFAP reactivity concomitant to the accumulation of LAMMs (Fig. 3A and B). Most interestingly, the border of the injury displayed a dense population of $GFAP^+$ astrocytes limiting the lesion, demonstrating the phenomenon of corralling in LPS induced dopaminergic degeneration (Fig. 3C).

A closer look at the GFAP anatomically enclosed, LPS-induced lesion site showed a densely packed LAMM area covering the entire injury (Fig. 4A). Image analysis comparison of LPS-injured and intact SNpc, using Voronoi partition or crystallization, showed a vast region of tiling at the lesion site (Fig. 4B) filling and compacting the injury. The 3D blended view also showed a honeycomb-like tiling at the LPS-targeted parenchyma (Fig. 4C) similar to morphologies previously reported for traumatic brain injury (Jassam et al., 2017). Cells were grouped membrane-to-membrane along the SNpc most probably participating in the phagocytic clearance of debris.

Because phagocytosis may be critical for injury healing of LPS-mediated dopaminergic elimination, we analyzed with high-resolution detail the phagocytic capacity of LAMMs at the rats' lesion sites. First, we identified a constellation pattern of TH^+ material in the LPS lesion area, with barely recognizable dopaminergic neuronal bodies (Fig. 5A). Alpha blending and 3D reconstructions revealed a large amount of TH^+ debris, within the volumetric space of the lesion, some of which was contained inside $OX42^+$ LAMMs (Fig. 5B). Certain TH^+ material was identifiable as neuronal bodies completely surrounded by LAMMs (Fig. 5C and Supplementary video 1). High-resolution confocal Z scans confirmed that TH^+ material was completely engulfed by LAMMs at the injection site, and 3D reconstructions facilitated the visualization of these phagocytic events (Fig. 5D, E, and Supplementary video 2). Interestingly, the volume of TH^+ debris, although reduced, persisted even seven days after the lesion (Supplementary Fig. S2) together with an important volumetric reduction of $OX42^+$ membranes (Supplementary Fig. S2), indicating a slow and prolonged initiation of the wound healing process.

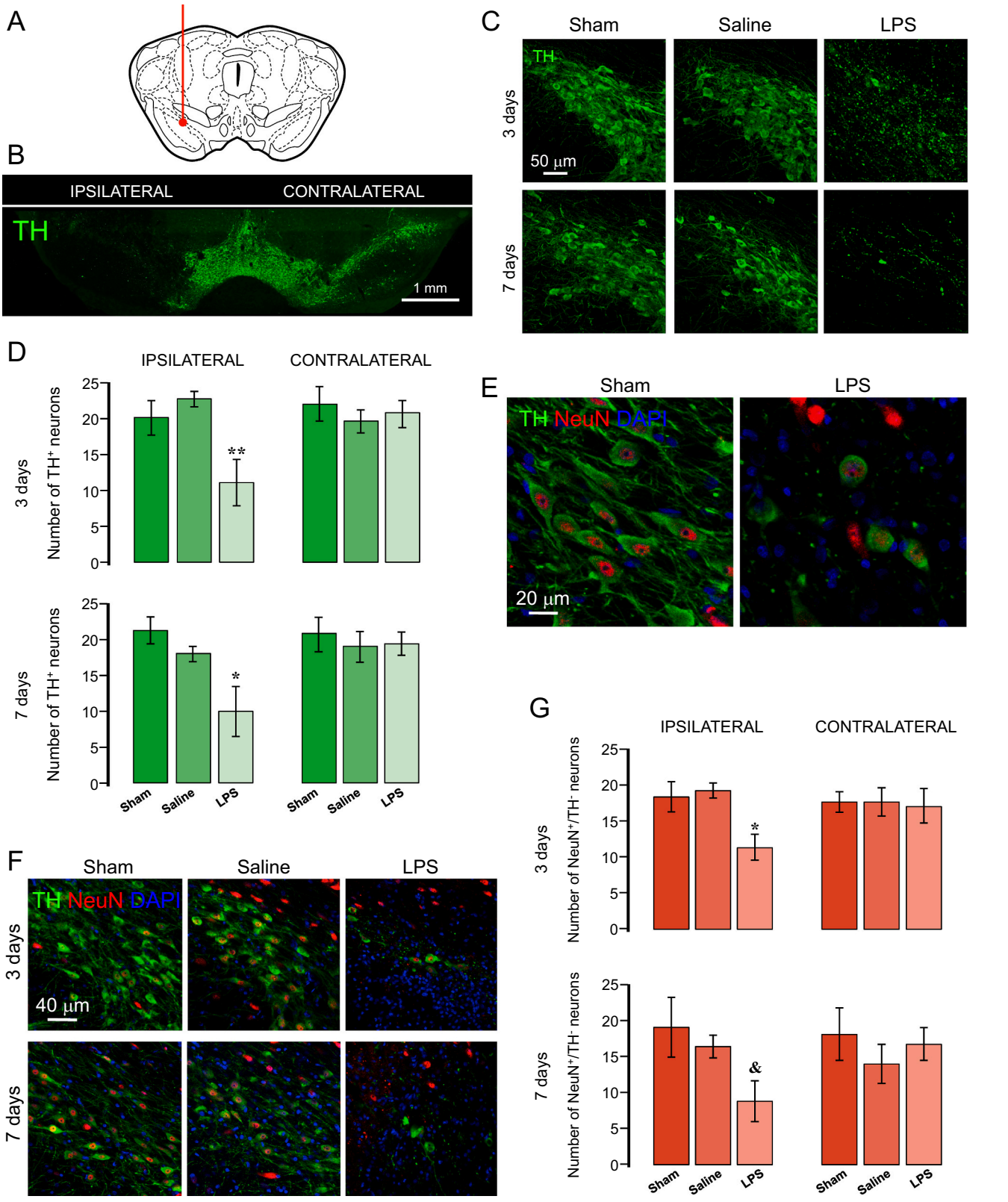

Fig. 1. Intracranial injection of LPS induces lasting dopaminergic and non-dopaminergic neuronal loss. A. Diagram of the injection site in rat brain section. B. Photomosaic of a representative LPS-injected section at SNpc level with TH immunofluorescence. C. Representative confocal images of TH loss in the experimental groups. D. Quantification of dopaminergic neurons in ipsilateral and contralateral side, three and seven days after LPS injection. E. Representative high-resolution confocal images of immunofluorescence for TH (green) and NeuN (red) combined with DAPI (blue) counterstaining in intact and LPS injected SNpc (3 days after intracranial injection). F. Representative comparison of TH/NeuN in all experimental groups. G. Quantification of non-dopaminergic ($NeuN^{+}/TH^{-}$) neurons in the SNpc, three and seven days after the injection. $^{*}p < 0.05$, $^{**}p < 0.005$ with respect to sham or $\&p < 0.05$ to saline. Six animals were analyzed per group. (For interpretation of the references to colour in this figure legend, the reader is referred to the web version of this article.)

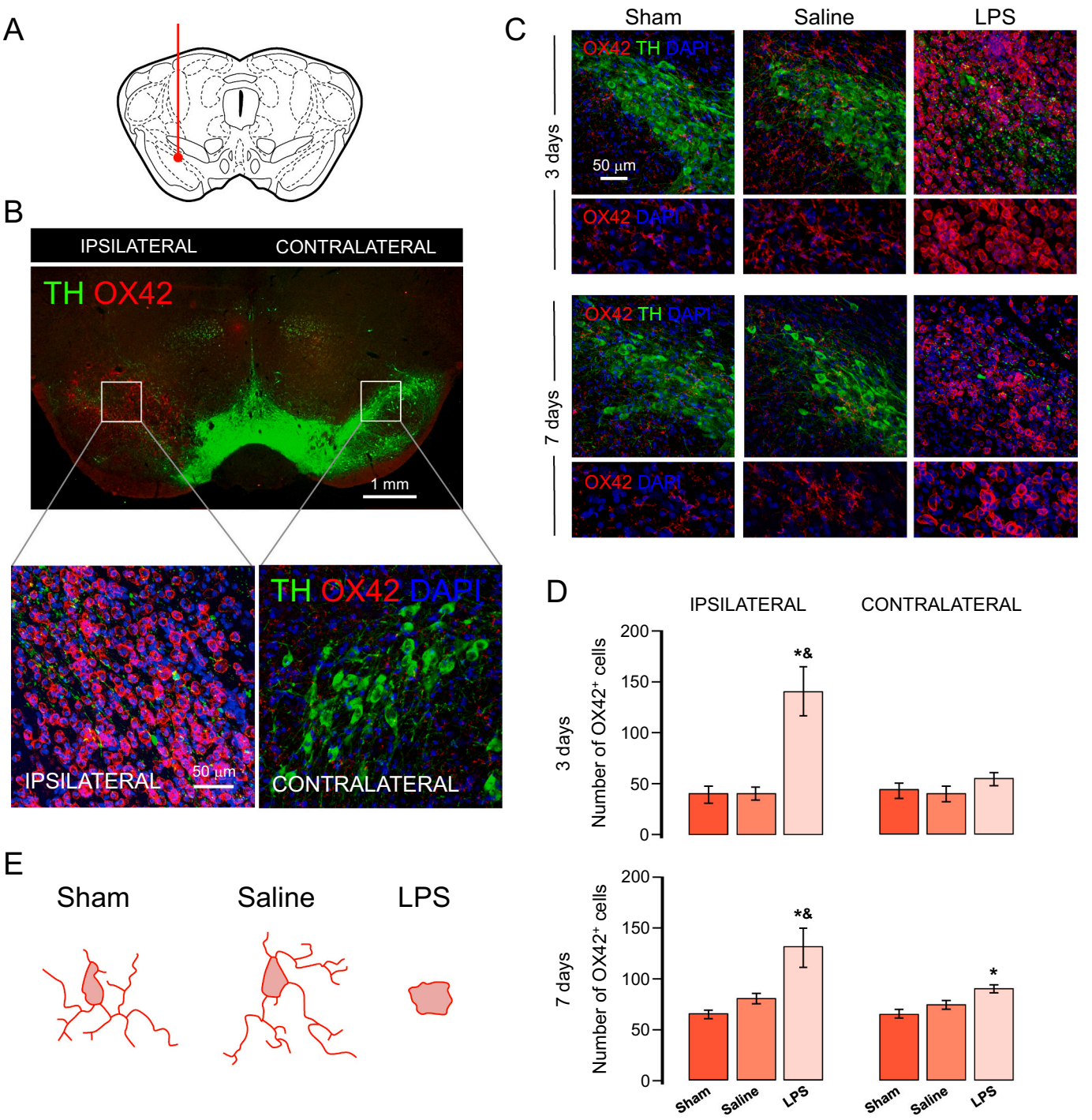

Fig. 2. LAMMs massively populate LPS-induced dopaminergic lesion. A. Diagram of a representative rat brain section illustrating the location of the injection site applied to the SNpc. B. Photomosaic of section at the SNpc displaying the differences between the injected site (ipsilateral) and the non-injected site (contralateral) evidenced by immunofluorescence for TH and OX42. Representative confocal images from insets illustrating the contralateral and ipsilateral view in higher resolution, evidenced by immunofluorescence for TH and OX42, and DAPI as a counterstaining are also shown. C. Representative images of OX42 expression in the SNpc of the three groups of animals (Sham, Saline and LPS), at the same anatomical level of the previous fig. D. Stereological quantification of OX42-expressing cells in the analyzed groups (3 days and 7 days after intracranial injections). *$p < 0.001$ with respect to sham; &$p < 0.001$ with respect to saline. E. Skeletonized diagrams of representative OX42$^+$ cell morphology in the SNpc of the three experimental groups. Six animals were analyzed per group.

In addition, although rare events, pyknotic nuclei could be seen inside OX42$^+$ cells, suggesting potential instances of primary phagocytosis (Fig. 5F). Quantification of phagocytic events revealed high phagocytic activity at three days with a significant reduction of phagocytic events seven days after the lesion (Fig. 5G), indicating the evolving resolution of the injury. However, persistent phagocytic activity of LAMMs after LPS lesion was still detectable seven days after the injection with similar percentage of phagocytizing as on day three (Fig. 5G) evincing that elimination of dopaminergic cell fragments is a long-lasting process during the course of the wound healing.

Because LPS injection caused a dramatic dopaminergic neuronal loss accompanied by a massive LAMM corralling in tissue, we designed an *in vitro* platform to understand the initial roles of microglial-mediated neuroinflammation in the primary stages of this scenario. First, to

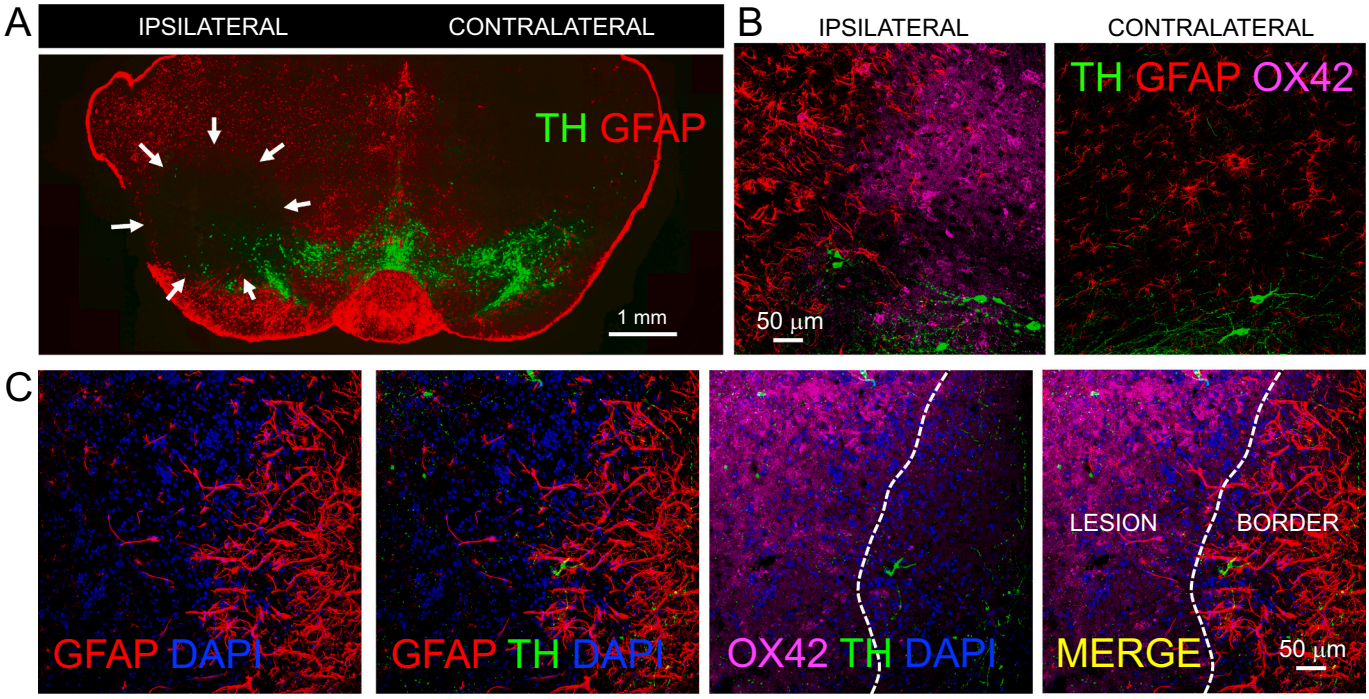

Fig. 3. LPS-induced lesion induces GFAP astrocytic corraling in the SNpc. A. Composite mosaic of the mesencephalon of a representative LPS-injected rat shows GFAP overreactivity (red) corraling the lesion (limited by white arrows) at the ipsilateral hemisphere compared with contralateral side. Dopaminergic neurons (green) are also labeled with TH antibodies (representative image from 3 days after intracranial injection). B. Zoom-in micrography at the border of the lesion shows highly overreactive astrocytes limiting an area denselly populated by $OX42^+$ cells (magenta). Contralateral side, at the same anatomical location, is also shown. C. Z confocal scan at the border reveals the high GFAP expression at the border compared with the site of the LPS lesion. $DAPI^+$ nuclei (blue), TH^+ dopaminergic neurons (green) and $OX42^+$ LAMMs are also labeled (magenta). (For interpretation of the references to colour in this figure legend, the reader is referred to the web version of this article.)

determine the direct toxicity of LPS, we treated dopaminergic cells with increasing concentrations, and we observed only a slight dopaminergic cell loss in some instances (Fig. 6A). Next, we separately treated microglia with the same protocol, detecting an increase in cell numbers, but a relatively low or absent inflammatory response as determined by nitrite release and microglial cell size (Fig. 6B-D).

Since a sole LPS administration does not explain the dramatic dopaminergic cell elimination, we co-cultured microglia and dopaminergic cells to determine the role of the intercellular interactions. We observed a dramatic loss when combining both cell types (Fig. 6E-H), with no apparent changes when adding increasing LPS concentrations, demonstrating that the presence of microglia appears to be essential for LPS-induced dopaminergic cell elimination (Fig. 6I and J) in the initial phases of pro-inflammatory injury.

Because this microglial-mediated elimination was spontaneous in this setting and apparently without an evident neuro-inflammatory stimulus, we wanted to confirm that the interaction with PC12 dopaminergic cells *in vitro* does not trigger an inflammatory response. To do so, we analyzed microglial activation following PC12 presentation and compared it with the canonical proinflammatory stimulus LPS and IFN-γ. The LPS/IFN-γ combination increased microglial activation parameters in contrast with interaction solely with PC12, demonstrating that the encounter with dopaminergic cells does not trigger this neuroinflammatory response (Fig. 7A-E).

Knowing that the presence of microglia is critical for the elimination of dopaminergic cells, we postulated that phagocytosis might be a major event in eliminating dopaminergic cell targets or debris. However, to understand the importance of the microglial-mediated toxic environment, we cultured dopaminergic cells with supernatant coming from naïve or activated microglia, and we observed a substantial reduction in dopaminergic cell numbers when adding supernatant from naïve and LPS/IFN-γ-activated microglia, demonstrating that the toxic environment is also crucial for neuroinflammatory-mediated dopaminergic elimination (Fig. 7F-I).

3. Discussion

In the present study, we show that LPS is an efficient compound producing a lesion in the brain parenchyma that effectively depletes mesencephalic neurons. Parallel to this lesion, a massive LAMM activation occurs within the wounded area, populating the entire lesion membrane-to-membrane and showing persistent phagocytosis of dopaminergic debris. Importantly, the lesion shows the phenomenon of corralling, surrounded by a continuous palisade of reactive astrocytes. This wound compaction scenario juxtaposes the inflammatory landscape seen in ageing and PD (McGeer et al., 1988) or MPTP insult in humans and non-human primates (Barcia et al., 2004; Langston et al., 1999), where microglial cells appear activated within a preserved and recognizable nerve tissue structure. It is also different from the display of reactive astrocytes described in PD, which appear diffused throughout the SNpc and without displaying corralling (McGeer and McGeer, 2008). In the case of rodent PD models, although a tangential infiltration of monocytes/macrophages may be found, the anatomical architecture of the parenchyma is not severely affected. MPTP insult in mice only causes an early (24 h) and transient monocyte infiltration not altering the outcome of dopaminergic degeneration (Parillaud et al., 2017), microglia being the main cell phagocytizing dopaminergic neurons (Depboylu et al., 2012). In 6-OHDA-injected rats, the situation is quite similar (Akiyama and McGeer, 1989; Marinova-Mutafchieva et al., 2009), with a preserved structure and limited monocyte infiltration (Espinosa-Oliva et al., 2014). By contrast, the infiltration of monocytes/macrophages by intranigral injection of LPS appears to be relevant, and it has been previously identified (Bok et al., 2018; Flores-Martinez et al., 2018; Herrera et al., 2000), playing a central role in the LPS-dependent

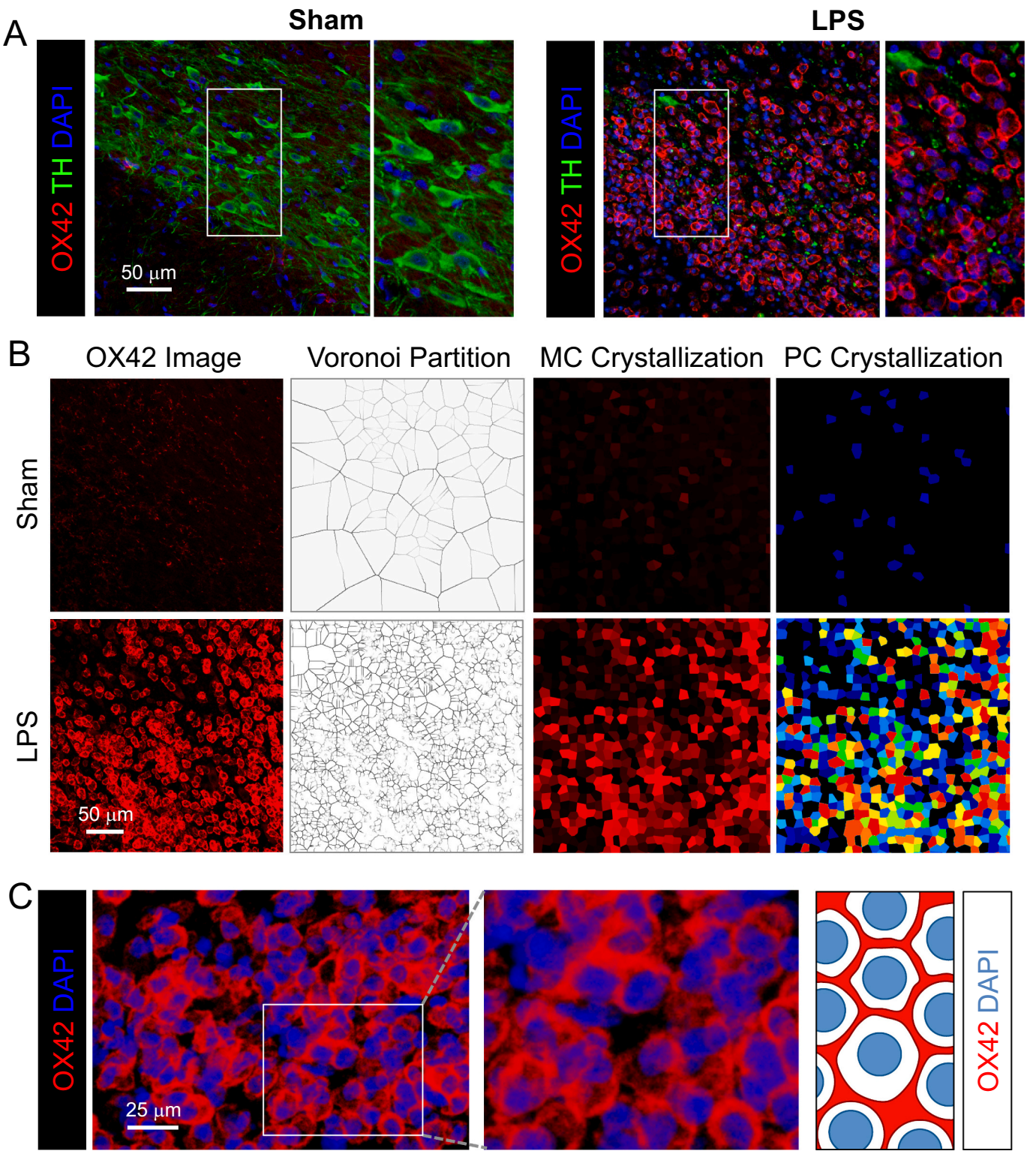

Fig. 4. LAMM corralling generates honeycomb tiling at dopaminergic lesion site. A. Massive OX42^{+} (red) LAMM colonization of LPS-induced dopaminergic lesion in the SNpc (LPS) compared to an intact animal (Sham) (3 days after intracranial injection). Dopaminergic neurons are evidenced by TH (green) and nuclei (blue) are also counterstained (DAPI). B. Voronoi partition, monochrome (MC) and polychrome (PC) crystallization of OX42 images reveal dense tiling covering the injured areas in LPS-injected animals. C. LAMMs build a honeycomb-like tiling at lesion sites. Confocal images of OX42 cells (red) and DAPI^{+} nucleus (blue) are shown. Panel on the right illustrates the membrane-to-membrane apposition of OX42^{+} LAMMs at the SNpc. (For interpretation of the references to colour in this figure legend, the reader is referred to the web version of this article.)

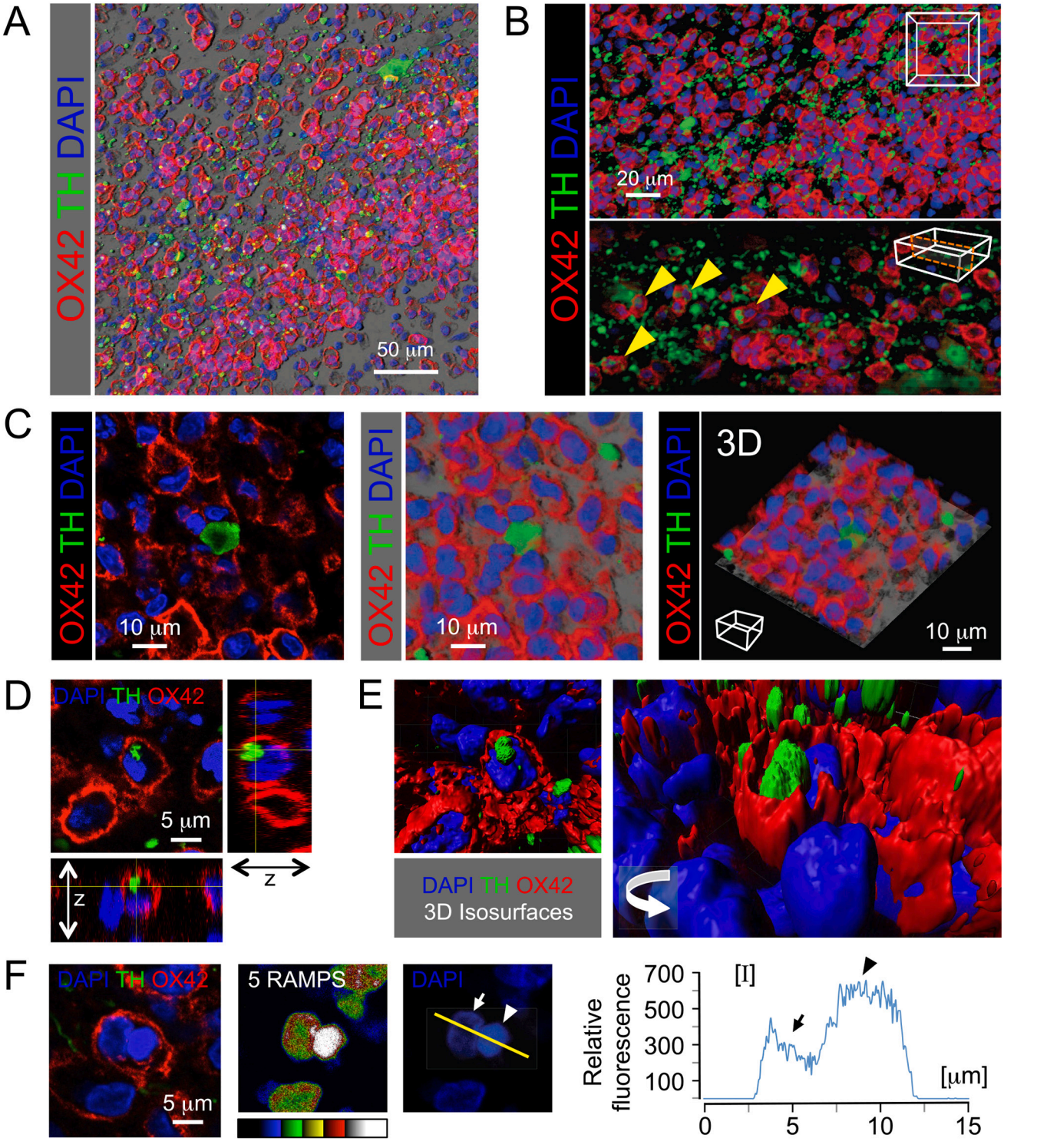

(caption on next page)

Fig. 5. LAMMs exhibit persistent debris phagocytosis at LPS-injected site. A. Shadowed blend view of OX42/TH/DAPI confocal 3D capture at LPS-injected SNpc (3 days after intracranial injection). B. Top panel shows a 3D blend view at the LPS-injected SNpc. Bottom panel shows rotated higher magnification of tissue block across a central clipping plane displaying multiple phagocytic events (some examples are indicated with yellow arrowheads). C. On the left, high magnification confocal slide at lesion site showing dopaminergic neuronal debris. Central panel shows shadowed blend view evidencing dopaminergic debris inside and outside OX42 cells. Right panel shows the same image as a 3D rotation view at the lesion. D. High resolution confocal plane and lateral views at z axis, evidencing complete engulfing of TH debris by a $OX42^{+}$ cell in the SNpc. E. Volumetric isosurface generation and rendering of the event showed in D, rotated and magnified on the right image. F. Confocal image of an $OX42^{+}$ cell containing a pyknotic nucleus, evidenced by 5 Ramps scale. Measurement of relative fluorescence of both nuclei at the yellow line (Arrow indicates normal nucleus and arrowhead indicates pyknotic nucleus). G. Quantification of phagocytic events and percentage of OX42 phagocytizing at the LPS-lesioned SNpc. $*p < 0.05$. Six animals were analyzed per group. (For interpretation of the references to colour in this figure legend, the reader is referred to the web version of this article.)

neuroinflammatory response in this anatomical area.

Although previous reports highlight the utility of using the direct LPS injection to the rat's SNpc (Herrera et al., 2000), because of the evident inflammatory response, the parallelism with PD is still questionable. The direct contact of LPS with the nerve tissue generates an inflammatory-mediated damage that significantly deteriorates the parenchymal structure. The resulting injury is so severe that some other structural proteins such as GFAP may not even be detected at the lesion core (Herrera et al., 2000). This is in fact compatible with our results in which GFAP reactivity is patent at the border of the injury but very limited at the lesion core. Thus, a fair comparison between 6-OHDA and LPS injection is hard to convey. The only report comparing both models uses an indirect approach, studying the LPS-induced neuroinflammation in the SNpc after a striatal injection (Parra et al., 2020). This is probably a more adequate approach for a PD-like inflammatory reaction since injecting into the striatum avoids the direct damage caused by LPS in the SNpc but generates an indirect microglial activation while structurally preserving the area of interest (Deng et al., 2020). Besides, this approach may also better match the potential indirect access of LPS, or other bacterial-derived components, to the brain parenchyma (Wong, 2021). Although in the present study we used a standardize LPS dose, we suggest that future studies may require adjusting the intracranial LPS dosage according to the manufacturers batch, to better establish the usefulness of this model for PD research.

The phagocytic process observed is also very different between the classical PD models and LPS. MPTP in mice induces a very specific reaction against intoxicated dopaminergic neurons engulfing entire neuronal bodies, enclosing pyknotic nuclei (Barcia et al., 2012). In contrast, in our images here, the phagocytosis of pyknotic nuclei is rare. Rather, constellations of dopaminergic debris, which are not observable after MPTP, are being phagocytized by a large number of LAMMs in a process of clearance.

Although the damage generated by direct LPS injection is patent, the mechanisms by which it occurs are to be further investigated. Parallel to traumatic brain injury, different phases may take place, including the initial phases, spanning minutes to hours, in which primary and secondary damage occur followed by a subsequent phase of resolution, covering several days (Jassam et al., 2017). Our co-cultures shed some light on this phenomenon, at least in the initial phases of the damage, indicating that sole delivery of LPS does not fully explain the dopaminergic toxicity, but requires the interaction of microglia for effective elimination. Probably, the presence of TLR4 receptors in myeloid cells may in part clarify this outcome, microglia being the major TLR4-expressing cell in the nerve tissue in contrast with neurons (Lehnardt et al., 2002). This is consistent with the idea that a massive LPS delivery within the CNS parenchyma triggers a LAMM-mediated inflammation that at first causes a large neuronal loss. This elimination may occur with the combination of cytotoxicity and phagocytosis, as supported by the *in vitro* results. This indicates that, initially, the exacerbated response of the host is key to the elimination of neurons rather than the direct toxicity of the endotoxin, consistent with previous reports (Brown, 2019; Bryant et al., 2010). This is coherent with previous reports where the depletion of LAMMs by clodronate reduces the severity of LPS-induced brain lesion in rodents (Lund et al., 2017; Zito et al., 2001), which appears particularly relevant in early time windows (Sheppard et al., 2019).

Then, in subsequent phases, our results pinpoint phagocytosis as part of the wound compaction and healing of direct LPS-dependent lesion in the CNS. Consistent with our *in vivo* images, this phagocytosis is evident and abundant three days after the lesion and, although reduced, remains persistent at least seven days after the LPS insult. Besides, the fact that $OX42^{+}$ cells completely surround dopaminergic neurons may also be interpreted as protective role in these phases of the injury resolution.

In this scenario, it seems that microglial-mediated neuroinflammation, combining cytotoxicity and phagocytosis, is essential for the dopaminergic elimination induced by LPS. However, the direct injection of LPS into the CNS generates such a massive wound, promoting corralling, which significantly alters the structure of the tissue and puts in question the parallelism with the idiopathic parkinsonian inflammatory response. This group of characteristics seems to be far from the PD-like inflammation, rather being similar to other recently described scenarios for massive nerve tissue lesions, where clearance of debris, wound healing and compaction, mediated by LAMMs, contribute to the tissue repair (Zhou et al., 2020).

In conclusion, our results demonstrate that direct LPS-mediated lesion in the SNpc triggers a massive inflammatory response, characterized by LAMM tiling and phagocytosis that contributes to the wound compaction and healing. Although this model may be useful to generate a drastic depletion of dopaminergic neurons, conclusions regarding the contribution of neuroinflammation in PD should be drawn cautiously. Novel approaches and techniques need to be further explored and modeled to better understand the neuroinflammatory contribution to dopaminergic neurodegeneration in PD.

4. Materials and methods

4.1. Animals and surgeries

Thirty-six adult male Wistar rats (200–300 g, 2.5 months) were used for this study. Rats were housed in Plexiglas cages (33 × 44 × 20 cm) at the animal housing facilities ($n = 5$ per cage) under a 12/12 h light/dark cycle (light on at 08:00) at room temperature (RT) with water and food *ad libitum*. All experimental procedures were performed according to the International Guide for the Care and Use of Laboratory Animals (National Research Council, 2011), register # ICS-2017-007 and the study was approved by ethical committee of Instituto de Ciencias de la Salud from Universidad Veracruzana, and the NOM-062-ZOO-1999 and NOM-087-ECOL-SSA1–2002 from Mexican legislation. All efforts were made to minimize animal discomfort during the study. Two sets of experiments were planned according to the different time window between the intranigral injection of LPS and the euthanasia. In addition to a sham group, rats were injected either with an intracranial injection of LPS or saline in the SNpc. The groups of animals were then perfused three ($n = 18$) or seven days (n = 18) after the LPS.

Three groups of animals ($n = 6$ per group) were used for each set of experiments: group 1 (n = 6): sham (dura mater removed); group 2 (n = 6): saline (saline solution intranigral injection) and group 3 (n = 6): LPS (intranigral LPS injection). Animals were injected intranigrally with 10 μg/2 μL of LPS or saline solution at the same volume. In summary, 36 rats were used for the histological assessment, 18 for each time point, distributed in groups of six animals.

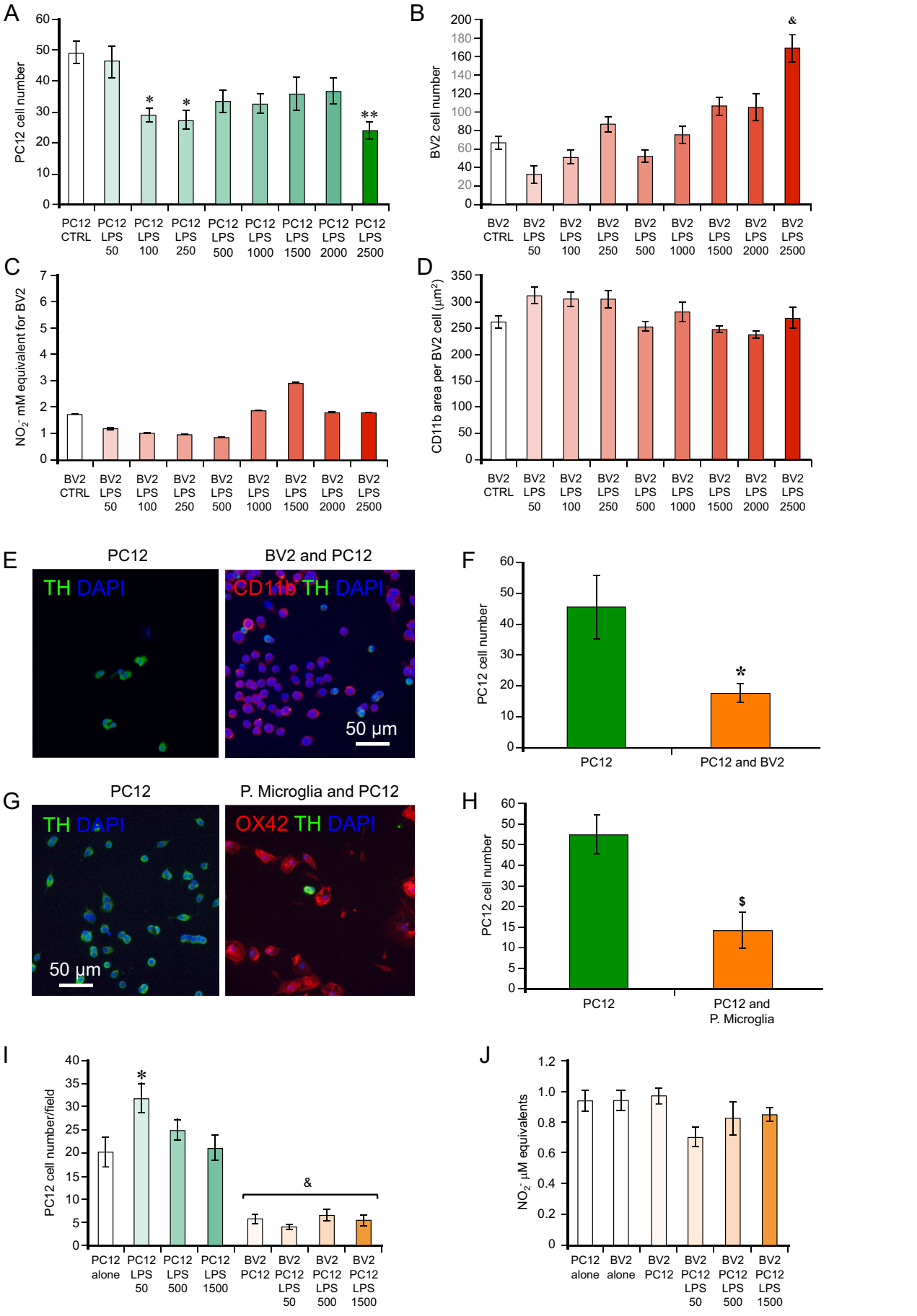

(caption on next page)

Fig. 6. LPS by itself is slightly toxic to PC12 dopaminergic cells and scarcely increases microglial-mediated neuro-inflammatory response while the presence of microglia spontaneously eliminates dopaminergic cells. A. Quantification of PC12 dopaminergic cell density after LPS treatment in cell culture. $*p < 0.01$ and $**p < 0.001$ with respect to CTRL. B. Quantification of microglial cell number after increasing concentrations of LPS. $\&p < 0.001$ with respect to the other conditions. C. Concentration of nitrites released by microglia after LPS treatment. No differences were seen with respect to CTRL. D. Quantification of CD11b expressing area in microglial cells after LPS treatment. No differences were seen with respect to the CTRL. E. Representative micrographies of dopaminergic cell culture, labeled with TH antibodies (green), before and after adding BV2 microglial cells, labeled with CD11b antibodies (red). DAPI was used as counterstaining. F. Quantification of PC12 dopaminergic cells before and after adding BV2 microglia. $*p < 0.05$ with respect to PC12 alone. G. Representative pictures of TH^+ dopaminergic cells (green), before and after adding primary microglia, labeled with OX42 antibodies (red) in combination with DAPI (blue). H. Quantification of TH+ cells before and after co-culture with primary microglia. $\$p < 001$, compared with PC12 alone. I. Quantification of dopaminergic cells after microglial presentation with increasing concentration of LPS. $*p < 0.01$ with respect to PC12 alone. $\&p < 0.001$ with respect to conditions without microglia. J. Quantification of nitrites release after LPS treatment (Analyses and quantifications were made after 24 h of treatment for each condition). No differences were seen between treatments. Each experiment had three replicates. (For interpretation of the references to colour in this figure legend, the reader is referred to the web version of this article.)

Intracranial surgery was done as follows. Rats were anesthetized with a single intraperitoneal dose of ketamine/xylazine (10 mg/kg/8 mg/kg) and received an intranigral injection of LPS from *Escherichia Coli* 055: B5) (Sigma-Aldrich; St. Louis, MO, USA) or saline. We used the following coordinates: AP +3.0 mm, from the interaural point; ML +2.8 mm from the intraparietal suture and DV -6.9 mm from the dura mater. The injection flow was 0.2 μL/min maintained by a perfusion micropump (Stoelting, Wood Dale, IL, USA) according to previous procedure (Hernandez-Baltazar et al., 2013). Once the LPS or saline solution was injected, according to each case, the needle was left inside five minutes to allow complete diffusion, then was withdrawn slowly after which the animals were sutured.

4.1.1. Perfusion

Three or seven days after surgery, animals were deeply anesthetized with 100 mg/kg i.p. of sodium pentobarbital (SedalPharma®, Laboratorios Pet's Pharma México), and perfused transcardially with 200 mL of 0.1 M PBS (from 1 M PBS, 8.1 mM Na2HPO4, 1.2 mM KH2PO4, 138 mM NaCl, 2.7 mM of KCl, filtered, pH 7.4) and with 100 mL of 4% paraformaldehyde in 0.1 M PBS using a peristaltic pump. During the perfusion, only the head of the animal was favored, so it was necessary to mechanically occlude the descending aortic artery.

4.1.2. Extraction of brain tissue

Once the perfusion was completed, the brains were immediately removed and post-fixed for 24 h at 4 °C in 4% paraformaldehyde. After this, they were placed in 30% sucrose solution in 0.1 M PBS under the same storage conditions. Subsequently, brains were cut in 35 μm-thick serial sections in a cryostat (Leica CM1520, Leica Inc., Germany) in coronal plane to obtain a representative sample of all levels of the SNpc. The 35 μm slices were collected starting from the anterior-most portion of the SNpc and sequentially placed with a soft-bristled brush inside a sterile 24-well box (Nalgene), previously filled with 0.1 M PBS. Sections were placed one by one in six series; this allowed 9–10 representative sections of SNpc to be obtained for each well. The tissue was stored in cryoprotective solution at −20 °C until used.

4.1.3. Immunofluorescence

Tissues were washed three times for 10 min with PBS containing 0.13 M NaCl, 0.010 M Na_2HPO_4 and 0.002 M NaH_2PO_4 at pH 7.4. Next, they were immersed in citrate buffer at 60–80 °C for 20 min and rinsed again with PBS for five minutes and after with TBS-Triton 0.05%. Subsequently, they were incubated for one hour in 10% horse serum +0.1% sodium azide for blocking nonspecific sites, then washed five minutes with horse serum 1% + sodium azide 0.1% and incubated with primary antibodies [anti-TH (rabbit, 1:1000) (Merck-Millipore, Darmstadt, Germany) for identification of dopaminergic neurons; anti-OX42 (mouse, 1:500) (Abcam, Cambridge, United Kingdom) and Iba-1 (rabbit, 1:500) (Wako Chemicals, Hong Kong) for microglial cells; anti-NeuN (mouse, 1:300) (Merck Millipore, Darmstadt, Germany), to detect neuronal nuclei, and anti-GFAP (Chicken, 1:500) (Abcam, Cambridge, United Kingdom)] in 1% horse serum solution +0.1% sodium azide for 48 h at room temperature (RT). After that, three 10-min washes were done with TBS-Triton 0.05% and tissues were incubated with fluorescent secondary antibodies: Alexa Fluor 488 (goat anti-rabbit IgG) (Thermofisher, Waltham, MA, USA), Alexa Fluor 488 (goat anti-mouse IgG) (Thermofisher, Waltham, MA, USA) Alexa Fluor 555 (Goat anti Chicken Ig) (Thermofisher, Waltham, MA, USA), and Alexa Fluor 555 goat anti-mouse IgG (Thermofisher, Waltham, MA, USA), for four hours (at a concentration of 1:1000 in horse serum 1% + sodium azide 0.1%) and protected from light. Next, three washes were done with PBS for 10 min and tissues were incubated with DAPI (1:1000) (Thermofisher, Waltham, MA, USA), for 30 min to label the cell nuclei. They were rinsed with PBS three times for 10 min and finally were mounted on non-gelatinized slides and protected with antifading reagent (Pro-Long Gold, Thermofisher, Waltham, MA, USA) and coverslips.

4.2. Image capture and quantifications

TH and Iba-1 immunoreactivity were visualized under the multichannel epifluorescence microscope (Eclipse 90i, Nikon), adapted to a high-resolution camera (Nikon DXM1200F), using software to systematically capture images (ACT-1). Representative mosaic images of the SNpc were also taken with a high-resolution camera with a microscope with an automated stage (Eclipse TE2000-E, Nikon) covering the section with systematic images according to x and y coordinates. Image mosaics were built using a stitching tool plugin (Image J). The number of cells was quantified using a specialized software (Image J) and considering the physical dissector as stereological criteria. Three representative sections of the mesencephalon containing the SNpc were imaged, and nine sampling dissectors covering the SNpc were quantified per hemisphere. Each dissector was quantified with the inclusion and exclusion criterion according to previous protocols (Gundersen, 1986).

4.3. Confocal microscopy

TH/OX42 and TH/NeuN positive cells were visualized using a high-resolution confocal microscope (Zeiss LSM 700) with a 20× objective and capturing systematic images of the SNpc with specialized software (ZEN 2010, Zeiss). For quantifications, $TH^+/OX42^+$ or $TH^+/NeuN^+$ immunofluorescence images were captured in 3D stacks configured with several optical sections with a 1-μm optical interval and analyzed with specialized software. In addition, DAPI was also captured as counterstaining. For numerical quantifications, including number of cells and the number phagocytic events, we used object counter tools (Image J) and optical dissector stereological criteria. To quantify volumes and visualize phagocytosis events, we used different three-dimensional rendering software (Imaris, Bitplane and Illucida FX, Los Angeles) to create isosurfaces and blend views. To visualize Voronoi partition and crystallization, we also used specialized software applications (ImageJ and Pixelmator). Analysis and visualization of relative florescence with 5 ramps was also done with specific application software (Image J).

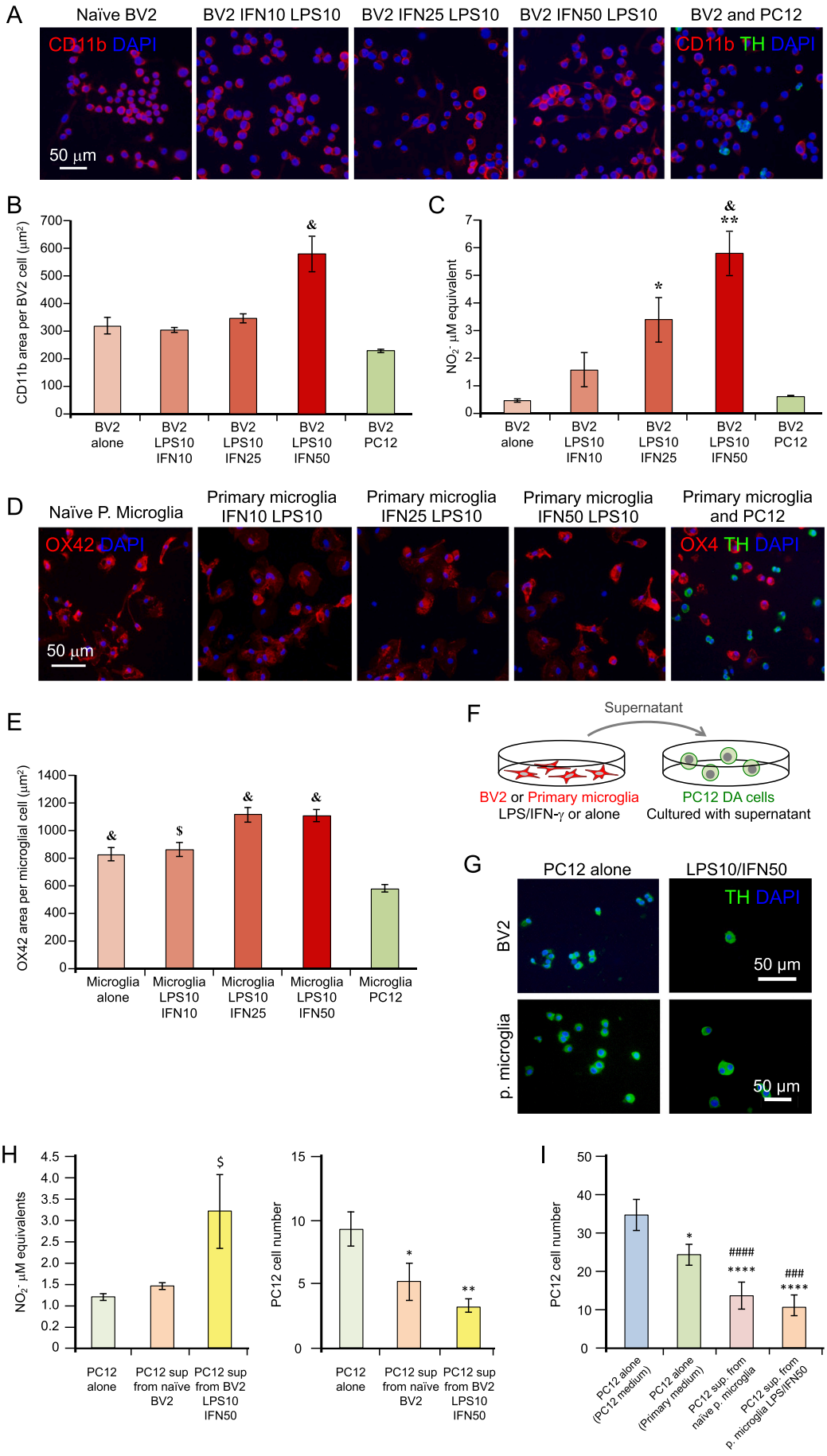

Fig. 7. Cytotoxicity from activated microglia is deleterious for dopaminergic cells. A. Presentation of PC12 dopaminergic cells does not activate BV2 microglia. Representative micrographies of cultured BV2 microglia after LPS with increasing concentrations of IFN-γ, or addition of PC12. B. Quantification of CD11b expressing area in BV2 microglia after treatments or PC12 presentation. &$p < 0.001$ with the rest of the conditions. C. Quantification of nitrites released by microglia after experimental conditions. *$p < 0.05$ and **$p < 0.001$ with respect to BV alone, &$p < 0.001$ with respect to PC12 with BV2. D. Representative pictures of mesencephalic primary microglia after LPS with increasing concentrations of IFN-γ, and co-cultures with dopaminergic cells PC12. E. Quantification of OX42 expresing area in primary microglia after treatments and interaction with PC12. $$p < 0.01$ &$p < 0.001$ with respect to Microglia-PC12. F. Diagram of the experimental design. G. Representative microscopy images of PC12 dopaminergic cells alone and after supernatant treatment from LPS/IFN-γ-treated microglia. H. Measurements of nitrites released in the experimental conditions (top chart), and quantification of dopaminergic cells after treatments. &$p < 0.05$ with respect to PC12 alone and sup from naïve. *$p < 0.05$ with respect to PC12 alone. **$p < 0.001$ with respect to PC12 alone. (Analyses and quantifications were made after 24 h of treatment for each condition). Each experiment had three replicates. I. Quantification of dopaminergic cells after treatment with media (either suited for PC12 or for primary microglia), supernatant from naïve or LPS/IFN-γ-treated primary microglia. *$p < 0.05$, ****$p < 0.001$ with respect to PC12 medium. ###$p < 0.01$, ####$p < 0.001$ with respect to primary medium.

5. Cell culture experiments

5.1. Cell lines

PC12 and BV2 cells were obtained from the INc-UAB institutional repository. BV2 is an immortalized murine microglia cell line, which has been widely used and successfully evaluated in response to LPS and IFN-γ (Henn et al., 2009). Both cell lines were maintained at 37 °C with 5% CO_2 in their corresponding media, which for the PC12 cell line was Dulbecco's Modified Eagle Medium (DMEM) (Ref#, 41,965,039, Thermofisher, Waltham, MA, USA) supplemented with 7% fetal bovine serum, 7% horse serum and 0.2% penicillin-streptomycin and for the BV2 cell line was Roswell Park Memorial Institute medium (RPMI) (Ref #, 21,875–034, Thermofisher, Waltham, MA, USA) supplemented with 10% fetal bovine serum and 0.1% penicillin- streptomycin. For the different experiments, PC12 and/or BV2 were placed in a 24-well culture plate and grown for 24 h then treated with different compounds such as LPS at different concentrations (from 50 ng/mL to 2500 ng/mL and 10 ng/mL when combined with IFN-γ), IFN-γ (from 10 ng/mL to 50 ng/mL), or co-cultured with PC12. The process to carrying out the BV2 microglial and PC12 dopaminergic cells *co*-culture started with plating BV2 in poly-L-lysine-coated coverslips in a 24-well culture plate in a concentration of 50.000cells/mL with 500 μL of DMEM medium. They were allowed to grow in an incubator at 36 °C and 5% of CO_2 for 24 h. BV2/PC12 co-culture was performed by the addition of PC12 cultured cells (500 μL) in a concentration of 100.000 cells/mL in the wells previously containing BV2 cell culture. Twenty-four hours after the treatment, the supernatant was collected to conduct the Griess assay or to treat subsequent cultures. At the end of the experiments, cells were fixed with 4% paraformaldehyde in PBS for immunocytofluorescence.

5.2. Primary cultures of midbrain microglia

Primary microglia was obtained from rats P0-P2 (OFA, Sprague Dawley). Rat pups were euthanized, and the midbrain was dissected and placed in a petri dish with PBS 1× supplemented with glucose. After this, a set of fresh solutions was prepared to get mixed glia from the midbrain. Solution 1 containing 50 mL Krebs 1×, 0.15 g BSA and 0.4 mL of Mg^{2+}, solution 2 combining 10 mL of solution 1 and 2.5 mg of trypsin, solution 3 prepared with 10 mL from solution 1, 0.8 mg DNase, 5.2 mg trypsine inhibitor and 0.1 mL Mg^{2+}, solution 4 prepared with 8.4 mL from solution 1 and 1.6 mL of solution 3, and, finally solution 5 containing 5 mL of solution 1, 40 μL of Mg^{2+} and 6 μL Ca^{2+}. Then, all collected midbrains were placed in solution 1 and centrifuged for 30 s at 1500 rpm, followed by suctioning the supernatant and adding solution 2 to the pellet, next, this was incubated at 37 °C for 10 min and later the solution 4 was added to the pellet together with solution 2, in order to proceed to the enzymatic digestion, afterwards tubes were spin at 1500 rpm. The supernatant was discarded, and 2–3 mL of solution 3 were added, then the cells were passed through a mesh to separate them. Finally, the rest of solution 3 was added through the mesh and all the content was added to solution 5, which was centrifuged at 1000 rpm for 5 min. After this, the supernatant was discarded and the pellet was re-suspended in 5 mL of mixed glia culture medium (DMEM medium, 10% fetal bovine serum and 1% penicillin-streptomycin). From this solution, 10 μL were taken and placed in an Eppendorf tube with 10 μL of tripan blue, and from the latter solution, 10 μL were taken and placed in a neubauer chamber to estimate the cell density. Cells were counted in order to add to the flask in a known concentration of mixed glia, in our case, 50,000 cells/mL. The rest of the volume of the flask was filled up with mixed glia culture medium. Once the mixed glia grew, the flask containing this glia was shaken at 300 rpm during 3 h, then the supernatant was collected to get the primary microglia since they grow in the superficial layers of the culture, consecutively primary microglia were placed in 24-well culture plate, letting the cells to grow up to 24 h. Then, they were treated with LPS and/or IFN-γ, or combined with PC12 cells at the same density mentioned for BV2-PC12 co-cultures, after 24 h cells were fixed with 4% paraformaldehyde in PBS for immunocytofluorescence. Analogously to BV2 cells, supernatant from naïve or LPS/IFN-γ-activated mesencephalic primary microglia was also used to treat PC12 cells.

5.3. Immunocytofluorescence

The immunocytofluorescence was performed on cell cultures to simultaneously detect TH and CD11b (in BV2) or OX42 (in primary microglia). Cells were washed with PBS, then permeabilized with 0.02% saponin/PBS at RT and later rewashed with PBS1×. Nonspecific sites were first blocked with PBS1×, 0.01% saponin and 0.075% glycine and later nonspecific sites were again blocked with PBS1×, 0.01% saponin, 0.075% glycine and 5% BSA. Coverslips containing the cells were placed in a humid chamber with 12 μL of PBS1×, 0.01% saponin, 1% BSA and the primary antibody overnight. To detect TH and CD11b, the primary antibodies were anti-TH (sheep, 1:500) (Merck; Darmstadt, Germany), anti-CD11b (rat, 1:1000) (Abcam; Cambridge, United Kingdom) and anti-OX42 (mouse, 1:500) (Abcam; Cambridge, United Kingdom), respectively. The following day coverslips were placed again in the 24-well plate, cells were washed with PBS 1X before being placed again in a humid chamber with PBS1X, 0.01% saponin, 1% BSA and the secondary antibody for 45 min. In order to detect TH, the secondary antibody was donkey anti-sheep (1:1000) in green fluorescence (Alexa Fluor 488) (Life Technologies; Carlsbad, CA, USA), for CD11b detection the secondary antibody was goat anti-rat (1:500) in red fluorescence (Alexa Fluor 555) (Bio-Rad Company; Berkeley, California, USA) and for OX42 goat anti-mouse (1:100) also in red fluorescence (Alexa Fluor 555) (Life Technologies; Carlsbad, CA, USA). Coverslips were later returned to the 24-well plate to be washed with PBS1X before adding 400 μL per well of the nucleus marker, DAPI (1:1000) (Life technologies; Carlsbad, CA, USA) in PBS1X. One more wash with PBS 1X was done before the coverslips were mounted on a glass slides using antifade reagent (Prolong Gold, Life Technologies; Carlsbad, CA, USA). For every experimental condition, a secondary antibody control was also performed, leaving one coverslip per condition without any primary antibodies.

5.4. Immunocytofluorescence quantification

To quantify the number of cells in the co-culture and its controls after treatments, we used an image analysis protocol. Each coverslip was imaged using a fluorescence microscope (Nikon Eclipse 90i) attached to a DXM 1200F digital camera and version 2.70 of the ACT-1 software (Nikon Corporation). With this system, we obtained 30 images per condition at 20×. Two quantification methods were used for the immunocytofluorescence labeling. One consisted of counting the number of cells, either PC12 or BV2, following stereological criteria and using a specialized software (Image J version 1.47, NIH, USA). The other method consisted of measuring the area of BV2 (CD11b) to estimate the activation, also using the same software (Image J version 1.47, NIH, USA).

5.5. Determination of nitrites by Griess assay

The determination of nitrites by Griess assay is based on a chemical reaction in which nitric oxide in the presence of an aromatic amine produces different compounds in sequence, resulting in a pink-colored compound, easily detectable by spectrophotometry. First, the calibration curve was prepared with known concentrations of $NaNO_2$ (100 μM, 50 μM, 25 μM, 12.5 μM, 6.25 μM, 3.125 μM, 1.5625 μM and 0.78125 μM), and 100 μL of each solution was added into a 96-well plate for the calibration curve, as was 100 μL of the experiment samples. Next, 100 μL of the Griess reagent (0.1 g in 2.5 mL milli-Q water) was added to every well. Duplicates were done for each condition. The plate was then incubated in darkness at RT for 15 min. Then the plate was read with specialized microplate reader software (KC Junior, Kansas City, MO,

USA) and the nitrite ion equivalents of the samples of interest were calculated according to the calibration curve prepared in the same 96-well plate.

5.6. Statistics

The results were expressed as mean ± standard error of the mean (SEM), which were calculated with suitable software (Sigma STAT or Excel, Microsoft Office MSO, Redmond, Washington, USA). All the data were statistically analyzed with suitable software (R commander package, R software; version 3.5.2, Free Software Foundation's GNU General Public License), using one-way analysis of variance (ANOVA) in pairwise comparisons of means mode. The value of $p < 0.05$ was the criterion to establish differences between means.

Supplementary data to this article can be found online at https://doi.org/10.1016/j.jneuroim.2022.577874.

Authors' contributions

PH, CR, PM, IF, AF, ES, PVC and MR performed the main research of this manuscript, including cell cultures and processing the samples for multilabeling, microscopy imaging, analyzing, and generating the 3D renderings. Importantly, PH conducted the brain surgeries and prepared the rat tissue samples. MJR, DH and CB designed and coordinated the research. The manuscript was written by CB and GP and revised and edited by all coauthors.

Ethics approval and consent to participate

All experimental procedures were performed according to the International Guide for the Care and Use of Laboratory Animals (National Institute of Health, 1999), register # ICS-2017-007 and the study was approved by ethical committee of Instituto de Ciencias de la Salud from Universidad Veracruzana, and the NOM-062-ZOO-1999 and NOM-087-ECOL-SSA1–2002 from Mexican legislation. The study was carried out in compliance with the ARRIVE guidelines.

Availability of data and materials

The data analyzed during the current study are available from the corresponding author on reasonable request.

Declaration of Competing Interest

The authors declare that they have no competing interests.

Acknowledgements

This project was supported by grants from the Spanish Ministry of Economy and Competitiveness, and the European Regional Development Fund (*Fondo Europeo de Desarrollo Regional*, FEDER) Reference Grants: RYC-2010-06729, SAF2013-45178-P, PEJ-2014-P00015, and SAF2015-64123-P, *Generalitat de Catalunya* (Reference Grant: 2014 SGR-984), Spanish Ministry of Science, Innovation and Universities (Reference Grant: PGC2018-096003-B-I00) for CBG; Project #17433201030 from *Universidad Veracruzana* for MJRH, *Cátedras* Project (Reference grant: 1840) for DHB and scholarship # 236573 for PHB from *Consejo Nacional de Ciencia y Tecnología* (CONACyT). We would like to thank all the personnel from the Administration and Technical Laboratories of the Institut de Neurociències, for the help provided at the Universitat Autònoma de Barcelona, with very special mention of the excellent technicians at the Microscopy Core, Núria Barba and Saioa Mendizuri and the Cell Culture Unit, Cristina Gutierrez, Antonio Cambero and Neus Ontiveros.

References

Akiyama, H., McGeer, P.L., 1989. Microglial response to 6-hydroxydopamine-induced substantia nigra lesions. Brain Res. 489, 247–253.
Barcia, C., Sanchez Bahillo, A., Fernandez-Villalba, E., Bautista, V., Poza, Y.P.M., Fernandez-Barreiro, A., et al., 2004. Evidence of active microglia in substantia nigra pars compacta of parkinsonian monkeys 1 year after MPTP exposure. Glia. 46, 402–409.
Barcia, C., Ros, C.M., Annese, V., Gomez, A., Ros-Bernal, F., Aguado-Yera, D., et al., 2011. IFN-gamma signaling, with the synergistic contribution of TNF-alpha, mediates cell specific microglial and astroglial activation in experimental models of Parkinson's disease. Cell Death Dis. 2, e142.
Barcia, C., Ros, C.M., Annese, V., Carrillo-de Sauvage, M.A., Ros-Bernal, F., Gomez, A., et al., 2012. ROCK/Cdc42-mediated microglial motility and gliapse formation lead to phagocytosis of degenerating dopaminergic neurons in vivo. Sci. Rep. 2, 809.
Bok, E., Chung, Y.C., Kim, K.-S., Baik, H.H., Shin, W.-H., Jin, B.K., 2018. Modulation of M1/M2 polarization by capsaicin contributes to the survival of dopaminergic neurons in the lipopolysaccharide-lesioned substantia nigra in vivo. Exp. Mol. Med. 50, 1–14.
Brown, G.C., 2019. The endotoxin hypothesis of neurodegeneration. J. Neuroinflammation 16, 180.
Bryant, C.E., Spring, D.R., Gangloff, M., Gay, N.J., 2010. The molecular basis of the host response to lipopolysaccharide. Nat. Rev. Microbiol. 8, 8–14.
Catorce, M.N., Gevorkian, G., 2016. LPS-induced murine neuroinflammation model: main features and suitability for pre-clinical assessment of nutraceuticals. Curr. Neuropharmacol. 14, 155–164.
Charvin, D., Medori, R., Hauser, R.A., Rascol, O., 2018. Therapeutic strategies for Parkinson disease: beyond dopaminergic drugs. Nat. Rev. Drug Discov. 17, 804–822.
Czlonkowska, A., Kohutnicka, M., Kurkowska-Jastrzebska, I., Czlonkowski, A., 1996. Microglial reaction in MPTP (1-methyl-4-phenyl-1,2,3,6-tetrahydropyridine) induced Parkinson's disease mice model. Neurodegeneration. 5, 137–143.
Deng, I., Corrigan, F., Zhai, G., Zhou, X., Bobrovskaya, L., 2020. Lipopolysaccharide animal models of Parkinson's disease: recent progress and relevance to clinical disease. Brain, Behav. Immun. Health. 4.
Depboylu, C., Stricker, S., Ghobril, J.P., Oertel, W.H., Priller, J., Hoglinger, G.U., 2012. Brain-resident microglia predominate over infiltrating myeloid cells in activation, phagocytosis and interaction with T-lymphocytes in the MPTP mouse model of Parkinson disease. Exp. Neurol. 238, 183–191.
Duty, S., Jenner, P., 2011. Animal models of Parkinson's disease: a source of novel treatments and clues to the cause of the disease. Br. J. Pharmacol. 164, 1357–1391.
Espinosa-Oliva, A.M., de Pablos, R.M., Sarmiento, M., Villaran, R.F., Carrillo-Jimenez, A., Santiago, M., et al., 2014. Role of dopamine in the recruitment of immune cells to the nigro-striatal dopaminergic structures. Neurotoxicology. 41, 89–101.
Flores-Martinez, Y.M., Fernandez-Parrilla, M.A., Ayala-Davila, J., Reyes-Corona, D., Blanco-Alvarez, V.M., Soto-Rojas, L.O., et al., 2018. Acute neuroinflammatory response in the substantia Nigra pars compacta of rats after a local injection of lipopolysaccharide. J Immunol Res 2018, 1838921.
Forno, L.S., DeLanney, L.E., Irwin, I., Monte, D.D., Langston, J.W., 1992. Chapter 36: Astrocytes and Parkinson's disease. In: ACH, Yu, Hertz, L., Norenberg, M.D., Syková, E., Waxman, S.G. (Eds.), Progress in Brain Research. Elsevier, pp. 429–436.
Gundersen, H.J., 1986. Stereology of arbitrary particles. A review of unbiased number and size estimators and the presentation of some new ones, in memory of William R. Thompson. J. Microsc. 143, 3–45.
Henn, A., Lund, S., Hedtjarn, M., Schrattenholz, A., Porzgen, P., Leist, M., 2009. The suitability of BV2 cells as alternative model system for primary microglia cultures or for animal experiments examining brain inflammation. Altex. 26, 83–94.
Hernandez-Baltazar, D., Mendoza-Garrido, M.E., Martinez-Fong, D., 2013. Activation of GSK-3β and Caspase-3 occurs in Nigral dopamine neurons during the development of apoptosis activated by a striatal injection of 6-Hydroxydopamine. PLoS One 8, e70951.
Herrera, A.J., Castaño, A., Venero, J.L., Cano, J., Machado, A., 2000. The single Intranigral injection of LPS as a new model for studying the selective effects of inflammatory reactions on dopaminergic system. Neurobiol. Dis. 7, 429–447.
Hirsch, E.C., Standaert, D.G., 2020. Ten unsolved questions about Neuroinflammation in Parkinson's disease. Mov. Disord. 36, 16–24.
Hoogland, I.C., Houbolt, C., van Westerloo, D.J., van Gool, W.A., van de Beek, D., 2015. Systemic inflammation and microglial activation: systematic review of animal experiments. J. Neuroinflammation 12, 114.
Jassam, Y.N., Izzy, S., Whalen, M., McGavern, D.B., El Khoury, J., 2017. Neuroimmunology of traumatic brain injury: time for a paradigm shift. Neuron. 95, 1246–1265.
Kalia, L.V., Lang, A.E., 2015. Parkinson's disease. Lancet. 386, 896–912.
Langston, J.W., Forno, L.S., Tetrud, J., Reeves, A.G., Kaplan, J.A., Karluk, D., 1999. Evidence of active nerve cell degeneration in the substantia nigra of humans years after 1-methyl-4-phenyl-1,2,3,6-tetrahydropyridine exposure. Ann. Neurol. 46, 598–605.
Lehnardt, S., Lachance, C., Patrizi, S., Lefebvre, S., Follett, P.L., Jensen, F.E., et al., 2002. The toll-like receptor TLR4 is necessary for lipopolysaccharide-induced oligodendrocyte injury in the CNS. J. Neurosci. 22, 2478–2486.
Lund, H., Pieber, M., Harris, R.A., 2017. Lessons learned about neurodegeneration from microglia and monocyte depletion studies. Front. Aging Neurosci. 9, 234.
Marinova-Mutafchieva, L., Sadeghian, M., Broom, L., Davis, J.B., Medhurst, A.D., Dexter, D.T., 2009. Relationship between microglial activation and dopaminergic neuronal loss in the substantia nigra: a time course study in a 6-hydroxydopamine model of Parkinson's disease. J. Neurochem. 110, 966–975.

McGeer, P.L., McGeer, E.G., 2008. Glial reactions in Parkinson's disease. Mov. Disord. 23, 474–483.
McGeer, P.L., Itagaki, S., Boyes, B.E., McGeer, E.G., 1988. Reactive microglia are positive for HLA-DR in the substantia nigra of Parkinson's and Alzheimer's disease brains. Neurology. 38, 1285–1291.
National Research Council, 2011. National Research Council (US) Committee for the Update of the Guide for the Care and Use of Laboratory Animals. Guide for the Care and Use of Laboratory Animals, 8th. National Academies Press (US), Washington, DC.
Orihuela, R., McPherson, C.A., Harry, G.J., 2016. Microglial M1/M2 polarization and metabolic states. Br. J. Pharmacol. 173, 649–665.
Parillaud, V.R., Lornet, G., Monnet, Y., Privat, A.L., Haddad, A.T., Brochard, V., et al., 2017. Analysis of monocyte infiltration in MPTP mice reveals that microglial CX3CR1 protects against neurotoxic over-induction of monocyte-attracting CCL2 by astrocytes. J. Neuroinflammation 14, 60.
Parra, I., Martinez, I., Ramirez-Garcia, G., Tizabi, Y., Mendieta, L., 2020. Differential effects of LPS and 6-OHDA on Microglia's morphology in rats: implications for inflammatory model of Parkinson's disease. Neurotox. Res. 37, 1–11.
Przedborski, S., 2017. The two-century journey of Parkinson disease research. Nat. Rev. Neurosci. 18, 251–259.
Romano, S., Savva, G.M., Bedarf, J.R., Charles, I.G., Hildebrand, F., Narbad, A., 2021. Meta-analysis of the Parkinson's disease gut microbiome suggests alterations linked to intestinal inflammation. NPJ Parkinsons Dis. 7, 27.
Schmid, C.D., Melchior, B., Masek, K., Puntambekar, S.S., Danielson, P.E., Lo, D.D., et al., 2009. Differential gene expression in LPS/IFNgamma activated microglia and macrophages: in vitro versus in vivo. J. Neurochem. 109 (Suppl. 1), 117–125.
Shapouri-Moghaddam, A., Mohammadian, S., Vazini, H., Taghadosi, M., Esmaeili, S.A., Mardani, F., et al., 2018. Macrophage plasticity, polarization, and function in health and disease. J. Cell. Physiol. 233, 6425–6440.
Sheppard, O., Coleman, M.P., Durrant, C.S., 2019. Lipopolysaccharide-induced neuroinflammation induces presynaptic disruption through a direct action on brain tissue involving microglia-derived interleukin 1 beta. J. Neuroinflammation 16, 106.
Tufekci, K.U., Genc, S., Genc, K., 2011. The endotoxin-induced neuroinflammation model of Parkinson's disease. Parkinsons Dis. 2011, 487450.
Wang, Q., Liu, Y., Zhou, J., 2015. Neuroinflammation in Parkinson's disease and its potential as therapeutic target. Transl Neurodegener. 4, 19.
Wong, W., 2021. A message for microglia from microbiota. Sci. Signal. 14, eabn3996.
Zhou, X., Wahane, S., Friedl, M.S., Kluge, M., Friedel, C.C., Avrampou, K., et al., 2020. Microglia and macrophages promote corralling, wound compaction and recovery after spinal cord injury via Plexin-B2. Nat. Neurosci. 23, 337–350.
Zhu, L., Zhao, Q., Yang, T., Ding, W., Zhao, Y., 2015. Cellular metabolism and macrophage functional polarization. Int. Rev. Immunol. 34, 82–100.
Zito, M.A., Koennecke, L.A., McAuliffe, M.J., McNally, B., van Rooijen, N., Heyes, M.P., 2001. Depletion of systemic macrophages by liposome-encapsulated clodronate attenuates striatal macrophage invasion and neurodegeneration following local endotoxin infusion in gerbils. Brain Res. 892, 13–26.